Boundary-Layer Meteorol (2014) 153:1–17
DOI 10.1007/s10546-014-9933-3

ARTICLE

A Boundary-Layer Scaling for Turbulent Katabatic Flow

Alan Shapiro · Evgeni Fedorovich

Received: 29 October 2013 / Accepted: 2 May 2014 / Published online: 25 June 2014

Abstract Scaling relationships are proposed for the turbulent katabatic flow of a stably stratified fluid down a homogeneously cooled planar slope—the turbulent analogue of a Prandtl-type slope flow. The Π Theorem predicts that such flows are controlled by three non-dimensional parameters: the slope angle, the Prandtl number, and a Reynolds number defined in terms of the surface thermal forcing (surface buoyancy or surface buoyancy flux), Brunt-Väisälä frequency, slope angle, and molecular viscosity and diffusivity coefficients. However, by exploiting the structure of the governing differential equations in a boundary-layer form, scaled equations are deduced that involve only two non-dimensional parameters: the Prandtl number and a modified Reynolds number. In the proposed scaling framework, the slope angle does not appear as an independent governing parameter, but merely acts as a stretching factor in the scales for the dependent and independent variables, and appears in the Reynolds number. Based on the boundary-layer analysis, we hypothesize that the full katabatic-flow problem is largely controlled by two rather than three parameters. Preliminary tests of the scaling hypothesis using data from direct numerical simulations provide encouraging results.

Keywords Direct numerical simulation · Katabatic flow · Planar slope · Stable stratification · Turbulence

1 Introduction: Katabatic Flow in the Prandtl Formulation

When a sloping surface is heated or cooled, a temperature difference arises between the near-surface air and the environmental air at the same altitude. The associated buoyancy force projects in the along-slope direction and induces a downslope flow over cooled surfaces (katabatic flow) or an upslope flow over heated surfaces (anabatic flow). Slope flows are

A. Shapiro (✉) · E. Fedorovich
School of Meteorology, University of Oklahoma, Norman, OK, USA
e-mail: ashapiro@ou.edu

A. Shapiro
Center for Analysis and Prediction of Storms, University of Oklahoma, Norman, OK, USA

ubiquitous in regions of complex terrain (Atkinson 1981; Whiteman 1990, 2000; Egger 1990; Poulos and Zhong 2008; Zardi and Whiteman 2012). Compared to anabatic flows, with well-mixed momentum and buoyancy profiles, katabatic flows have a more shallow, boundary-layer character.

Katabatic winds have wide-ranging impacts on weather and climate. In mid-latitudes they affect visibility, fog formation, air pollutant dispersion, agriculture, and energy use, as well as aerial spraying, controlled burning, and fire-fighting operations (Lu and Turco 1994; Raga et al. 1999; Whiteman 2000; Fernando et al. 2001; Hunt et al. 2003; Lee et al. 2003; Brazel et al. 2005; Fernando 2010; Steyn et al. 2012). Katabatic winds arising over the ice sheets of Greenland and Antarctica affect the weather and climate of the polar regions (Parish and Waight 1987; Parish 1992; Gallee and Schayes 1994; Oerlemans 1998; Heinemann and Klein 2002; Renfrew 2004; Renfrew and Anderson 2006). Katabatic flow from Antarctica drives sea ice offshore, exposing open water to the much colder atmosphere (Bromwich and Kurtz 1984; Bromwich 1989; Cotton and Michael 1994; Woert 1999). As this surface water refreezes, brine is rejected, leading to the production of vast amounts of dense sinking Antarctic Bottom Water, an important ingredient of the global ocean circulation (Adolphs and Wendler 1995; Bromwich et al. 1998; Massom et al. 1998; Williams et al. 2010; Barthélemy et al. 2012; Ohshima et al. 2013).

A major advance in the theory of slope flows was Prandtl's (1942) analytical description of the flow of a viscous stably stratified fluid along a uniformly heated or cooled planar surface. Prandtl considered an equilibrium state in which the along-slope advection of potential temperature balanced thermal diffusion, and the along-slope component of buoyancy balanced the viscous stress force. The balances were described in a remarkably simple one-dimensional framework[1] in which the dependent variables are functions only of the slope-normal coordinate Z. Prandtl's solution yielded the characteristic flow depth Z_P and jet speed U_P as

$$Z_P = \frac{(\nu_T \kappa_T)^{1/4}}{(N \sin\alpha)^{1/2}}, \tag{1a}$$

$$U_P = \frac{B|_{Z=0}}{Pr_T^{1/2} N}, \tag{1b}$$

where α is the slope angle, ν_T is the kinematic viscosity, κ_T is the thermal diffusivity, $Pr_T \equiv \nu_T/\kappa_T$ is the Prandtl number, $N \equiv \sqrt{(g/\Theta_r) d\Theta_e/dZ^*}$ is the Brunt-Väisälä frequency, $B \equiv g[\Theta - \Theta_e(Z*)]/\Theta_r$ is the buoyancy, Θ is the potential temperature, Z^* is the true height coordinate (the relation between Z^* and the slope-normal coordinate Z is depicted in Fig. 1), Θ_e is the environmental potential temperature, Θ_r is a constant reference value of potential temperature, and g is the acceleration due to gravity. The parameters α, ν_T, κ_T, and N are assumed to be constant; from the constancy of N it follows that Θ_e must vary linearly with Z^*.

Although Prandtl originally presented his solution in terms of laminar-flow variables, investigators who fit the Prandtl solution to data from real atmospheric flows invariably interpret ν_T and κ_T as effective turbulent transport (exchange) coefficients rather than as molecular coefficients. Because of this common usage, we have placed a subscript T (for turbulent exchange) on the diffusivities in our discussion of the Prandtl model. We also note

[1] The Prandtl solution for wind and buoyancy, together with pressure obtained from the quasi-hydrostatic equation (the equation to which the slope-normal equation of motion reduces in the one-dimensional framework), constitute an exact solution of the viscous Boussinesq equations of motion, thermal energy and mass conservation (incompressibility condition).

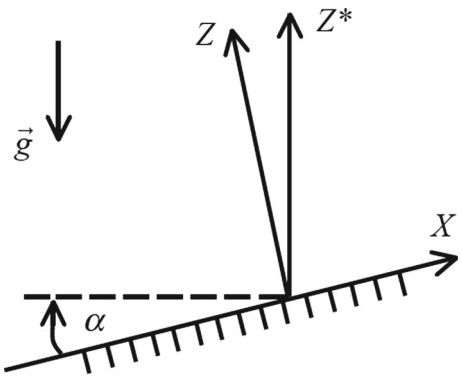

Fig. 1 Slope-following Cartesian coordinate system: the along-slope (X) and slope-normal (Z) axes are inclined at an angle α to the *horizontal* and *vertical* (Z^*) directions, respectively. The Y axis points into the page

that, although Prandtl considered the surface buoyancy to be specified, the solution is easily modified if the surface buoyancy flux is specified (Axelsen and van Dop 2009b; Fedorovich and Shapiro 2009a for $Pr = 1$; Mo 2013). In that case, Z_P is still given by (1a), but U_P varies as $N^{-3/2}(\sin\alpha)^{-1/2}$.

The Prandtl model with tuned exchange coefficients has provided qualitatively reasonable descriptions of mean-flow profiles in real katabatic flows (Defant 1949; Tyson 1968; Hootman and Blumen 1983; Clements et al. 1989; Papadopoulos et al. 1997; Oerlemans 1998), with the prediction of an increasing flow depth with decreasing slope angle confirmed by observations (Table 2.1 of Zardi and Whiteman 2012). However, because of the constancy of the exchange coefficients, the Prandtl model tends to underpredict the near-surface wind-speed and buoyancy gradients (Grisogono and Oerlemans 2001; Oerlemans and Grisogono 2002; Noppel and Fiedler 2002; Zammett and Fowler 2007; Axelsen and van Dop 2009b). In addition, a zone of weak return flow atop the katabatic jet in the Prandtl model is stronger, relative to the jet strength, than in numerical simulations or observations. Indeed, Zardi and Whiteman (2012) note that return flows associated with natural katabatic winds can be difficult to identify. By modifying the Prandtl model to include specified slope-normal variations in the exchange coefficients, Grisogono and Oerlemans (2001, 2002) and Parmhed et al. (2004) obtained improved wind-profile estimates under the Wentzel–Kramers–Brillouin (WKB) approximation.

Since microscale turbulent transport of heat, momentum, and moisture within katabatic flows cannot be explicitly described in mesoscale to global-scale atmospheric models, the effects of this transport are commonly parametrized. Unfortunately, the parametrization of stably stratified turbulence remains a difficult problem from both conceptual and technical standpoints (Mahrt 1998; Jiménez and Cuxart 2005; Mauritsen et al. 2007). The problem is even worse for stably stratified turbulence in slope flows for which a near-surface closure theory is still lacking (Burkholder et al. 2011).

Because of its conceptual compactness, the Prandtl model setting with uniform planar slope of infinite extent, spatially homogeneous thermal forcing, and stable stratification represented by a constant Brunt-Väisälä frequency, is an ideal departure point for studies of turbulent slope flows. In recent years, the powerful computational tools of large-eddy simulation (LES) and direct numerical simulation (DNS) have been applied to such flows. By resolving most of the energy-carrying motions, LES accounts for turbulence effects in a more accurate and consistent manner than is the case in mesoscale models, although it is still affected by the lack of a near-wall model that appropriately describes the interaction between shear and buoyancy forcings at the sloping boundary. In DNS, the governing equations are solved

directly, with turbulent motions simulated across all scales down to the dissipation scales, thus bypassing the need for closure models. High-fidelity DNS can provide benchmarks for many computational fluid dynamics problems, but involve a very high computational cost (Pope 2000). The computational burden is generally prohibitive for realistically high Reynolds numbers typical of geophysical applications. However, if one mitigates the cost by working with reduced Reynolds numbers, DNS can provide useful descriptions of flow structures within well-defined, albeit narrow, scale ranges.

The mean wind and buoyancy fields obtained in turbulent Prandtl-type slope flows via LES (Schumann 1990; Axelsen and van Dop 2009a, b; Burkholder et al. 2011; Grisogono and Axelsen 2012) and DNS (Fedorovich and Shapiro 2009a) were in good qualitative agreement with the Prandtl predictions. In particular, a tendency for flow depth to increase with decreasing slope angle was confirmed for both anabatic (Schumann 1990; Fedorovich and Shapiro 2009a), and katabatic (Axelsen and van Dop 2009b; Fedorovich and Shapiro 2009a) flows. Interestingly, the mean fields in Schumann's (1990) study exhibited temporal oscillations,[2] with a frequency close to $N \sin\alpha$, as in McNider's (1982) theory. Such oscillations were also found in the katabatic-flow simulations of Axelsen and van Dop (2009a, b) and Burkholder et al. (2011). In the latter study, several commonly used subgrid closure schemes for LES were evaluated *a posteriori* against the filtered results of DNS. While the closure models adequately reproduced low-order features such as mean winds and buoyancy, higher-order turbulence statistics were not properly predicted.

This study is concerned with scaling relationships for a turbulent analogue of Prandtl-type katabatic flows. In Sect. 2 we present the governing equations of the katabatic-flow problem and note that the Π theorem predicts a three-parameter space for their solution. In Sect. 3 we consider boundary-layer approximations to the problem and deduce scalings that reduce the boundary-layer problem to one governed by only two dimensionless parameters. We then hypothesize that the full katabatic-flow problem considered in Sect. 2 is essentially a two-parameter rather than three-parameter problem. Preliminary tests of this boundary-layer scaling hypothesis using DNS data are described in Sect. 4, with a summary and conclusions following in Sect. 5.

2 Governing Equations

Quiescent stably stratified fluid overlies a planar slope when, at time $T = 0$, a spatially homogeneous surface cooling is suddenly imposed and maintained thereafter. A turbulent katabatic flow develops along the surface in response to this cooling. The motion is considered in a slope-following right-hand Cartesian coordinate system (Fig. 1) with X, Y, and Z axes directed, respectively, up the slope, across the slope, and perpendicular to the slope. The governing equations are the Boussinesq equations of motion, thermal energy, and mass conservation (incompressibility condition) in the following forms[3] (Fedorovich and Shapiro 2009a),

$$\frac{\partial U}{\partial T} + U\frac{\partial U}{\partial X} + V\frac{\partial U}{\partial Y} + W\frac{\partial U}{\partial Z} = -\frac{\partial \Pi}{\partial X} + B\sin\alpha + \nu\left(\frac{\partial^2 U}{\partial X^2} + \frac{\partial^2 U}{\partial Y^2} + \frac{\partial^2 U}{\partial Z^2}\right), \quad (2)$$

$$\frac{\partial V}{\partial T} + U\frac{\partial V}{\partial X} + V\frac{\partial V}{\partial Y} + W\frac{\partial V}{\partial Z} = -\frac{\partial \Pi}{\partial Y} + \nu\left(\frac{\partial^2 V}{\partial X^2} + \frac{\partial^2 V}{\partial Y^2} + \frac{\partial^2 V}{\partial Z^2}\right), \quad (3)$$

[2] In Schumann (1990), as in the other LES/DNS studies cited above, the flow was generated from rest by the sudden application of a surface thermal perturbation (buoyancy or buoyancy flux).

[3] If the X-axis points downslope, the signs of the $\sin\alpha$ factors in (2) and (5) must be changed.

$$\frac{\partial W}{\partial T}+U\frac{\partial W}{\partial X}+V\frac{\partial W}{\partial Y}+W\frac{\partial W}{\partial Z}=-\frac{\partial \Pi}{\partial Z}+B\cos\alpha+\nu\left(\frac{\partial^2 W}{\partial X^2}+\frac{\partial^2 W}{\partial Y^2}+\frac{\partial^2 W}{\partial Z^2}\right), \quad (4)$$

$$\frac{\partial B}{\partial T}+U\frac{\partial B}{\partial X}+V\frac{\partial B}{\partial Y}+W\frac{\partial B}{\partial Z}=-UN^2\sin\alpha-WN^2\cos\alpha+\kappa\left(\frac{\partial^2 B}{\partial X^2}+\frac{\partial^2 B}{\partial Y^2}+\frac{\partial^2 B}{\partial Z^2}\right), \quad (5)$$

$$\frac{\partial U}{\partial X}+\frac{\partial V}{\partial Y}+\frac{\partial W}{\partial Z}=0. \quad (6)$$

Here, U, V, and W are the along-slope (X), cross-slope (Y), and slope-normal (Z) velocity components, respectively, $\Pi \equiv [P - P_e(Z^*)]/\rho_r$ is the normalized pressure perturbation, P is the pressure, $P_e(Z^*)$ is the environmental pressure, ρ_r is a constant reference value of density, ν is the (constant) molecular kinematic viscosity and κ is the (constant) molecular thermal diffusivity. Other quantities are as defined in Sect. 1. The first two terms on the right-hand side of Eq. 5 arise from the decomposition of the environmental potential temperature advection $-W^*N^2$ (where $W^* \equiv DZ^*/Dt$ is the true vertical velocity component) into along-slope and slope-normal components.

On the underlying sloping surface we apply no-slip, $U|_{Z=0} = V|_{Z=0} = 0$, and impermeability, $W|_{Z=0} = 0$, conditions, and impose either a spatially uniform buoyancy, $B|_{Z=0} < 0$, or buoyancy flux, $-\kappa(\partial B/\partial Z)|_{Z=0} = F_s (< 0)$. The latter can also be interpreted as a surface energy production rate. All dependent variables are considered to vanish as $Z \to \infty$.

We define a surface buoyancy scale B_s (> 0) either through the surface buoyancy or the surface buoyancy flux as

$$B_s \equiv \begin{cases} |B|_{Z=0}\,, & \text{(buoyancy-forced case)} \quad (7a) \\ H\left.\dfrac{\partial B}{\partial Z}\right|_{Z=0} = -\dfrac{F_s Pr^{1/4}}{\sqrt{\kappa N\sin\alpha}}, & \text{(flux-forced case)} \quad (7b) \end{cases}$$

where $Pr \equiv \nu/\kappa$ is the molecular Prandtl number and $H \equiv (\nu\kappa)^{1/4}/(N\sin\alpha)^{1/2}$ is the molecular analogue of the Prandtl depth scale Z_P. For future reference we also introduce the molecular analogue of the Prandtl velocity scale $U_P : V \equiv B_s/(Pr^{1/2}N)$.

The flow is governed by (2) to (6) and either (7a) or (7b). The dependent variables are functions of four independent variables (X, Y, Z, T) and five parameters (ν, κ, N, α, B_s). Since length and time are the only dimensions in this problem, the Π theorem (Langhaar 1951) predicts that any dimensionless (scaled) dependent variable is a function of the scaled versions of X, Y, Z, T and a non-unique set of three dimensionless parameters that may be chosen, for example, to be α, Pr, and $Re_U \equiv VH/\nu$.

3 Boundary-Layer Scaling

We suggest, tentatively, that scaling relationships for a turbulent katabatic flow, especially along shallow slopes, might be deduced from the boundary-layer-approximated governing equations. Our proposition is motivated by observational and theoretical studies pertaining to the inhibition of vertical motions by strong stable stratification and the promotion of layered, highly anisotropic flow structures with characteristic horizontal scales of motion being much larger than the vertical scales of motion (Hopfinger 1987; Wong and Griffiths 1999,Riley and Lelong 2000; Waite and Bartello 2004; Lindborg 2006). Remarkably, some experimental and theoretical studies of stratified turbulence suggest that such anisotropies may persist across the entire turbulence spectral range down to the smallest (dissipation) scales (Thoroddsen

and Van Atta 1992; Thoroddsen and Atta 1996; Werne and Fritts 2001; Pettersson Reif and Andreassen 2003; Godeferd and Staquet 2003).

We thus consider a set of approximations in which the X and Y derivatives in the viscous/diffusion terms are neglected in (2), (3), and (5), and the quasi-hydrostatic equation, $0 = -\partial\Pi/\partial Z + B\cos\alpha$, is used in place of (4). Analogous approximations are common in laminar fluid dynamics problems of boundary-layer type, for example, in the analysis of heat transfer in Blasius flow (Bejan 2013). It is important to note, however, that we are considering these approximations for equations governing a turbulent flow rather than a laminar flow. We will refer to the katabatic-wind problem subject to the above approximations as the boundary-layer problem. As in the full problem, the Π theorem predicts a three-parameter space for a description of the boundary-layer problem. However, as we will see below, by exploiting the structure of the boundary-layer equations, we may choose scales for the dependent and independent variables that convert the scaled boundary-layer problem to one governed by just two parameters. The scales are obtained by a formal procedure, and no claims are made regarding the relative magnitudes of any of the terms in the scaled boundary-layer problem.

We denote dimensionless (scaled) variables by lower-case letters as

$$(x, y) \equiv \frac{(X, Y)}{X_s},\ z \equiv \frac{Z}{Z_s},\ t \equiv \frac{T}{T_s},\ (u, v) \equiv \frac{(U, V)}{U_s},\ w \equiv \frac{W}{W_s},\ \pi \equiv \frac{\Pi}{\Pi_s},\ b \equiv \frac{B}{B_s}, \quad (8)$$

where B_s was defined in (7a) and (7b), and the scales X_s, Z_s, T_s, U_s, W_s, and Π_s have yet to be defined. To obtain these scales, we write each of them as an ansatz consisting of the product of powers of the dimensional parameters and also of powers of $\sin\alpha$ and $\cos\alpha$. We then apply (8) into the differential equations and boundary conditions for the boundary-layer problem and seek the ansatz exponents that yield as few independent parameters as possible in the scaled problem. From the Π theorem we know that we can obtain a three-parameter scaled problem, but we hope to do better than that by explicitly using the equations for the boundary-layer problem. Remarkably, we found that exponents could be chosen so that the slope angle α is completely removed as an independent parameter. In other words, the boundary-layer problem admits solutions that vary with slope angle in a structurally similar manner—α merely acts as a stretching factor. The scale-deduction procedure leads to the following scales:

$$\left.\begin{aligned} X_s &\equiv \frac{(\nu\kappa)^{1/4}\cos\alpha}{N^{1/2}\sin^{3/2}\alpha}, & Z_s &\equiv \frac{(\nu\kappa)^{1/4}}{(N\sin\alpha)^{1/2}}, & T_s &\equiv \frac{1}{Pr^{1/2}N\sin\alpha}, \\ U_s &\equiv \frac{B_s}{Pr^{1/2}N}, & W_s &\equiv \frac{B_s\tan\alpha}{Pr^{1/2}N}, & \Pi_s &\equiv \frac{B_s(\nu\kappa)^{1/4}\cos\alpha}{(N\sin\alpha)^{1/2}}. \end{aligned}\right\} \quad (9)$$

These scales (except for T_s) were used in Shapiro et al. (2012) as formal non-dimensionalization factors to yield the fewest parameters in a linear analysis of steady katabatic flow induced by a cold strip of finite width running across the slope. The scales Z_s and U_s (which are the same as the scales H and V defined in Sect. 2) are the molecular coefficient analogues of the characteristic flow depth and jet speeds Z_P and U_P in the Prandtl model. The scale X_s can be interpreted as the along-slope distance along which the elevation changes by the same amount as over the slope-normal distance Z_s (see Fig. 2 in Shapiro et al. 2012), although its relevance for characterizing the length of any flow feature is uncertain. Apart from the $Pr^{1/2}$ factor, $2\pi/T_s$ characterizes the natural frequency of internal gravity oscillations arising in linear and non-linear analytical slope-flow models (McNider 1982; Shapiro and Fedorovich 2007). Frequencies close to this natural frequency have been observed in nature and in numerically simulated slope flows (McNider 1982; Schumann 1990; Bastin and Drobinski 2005; Shapiro and Fedorovich 2007; Princevac et al. 2008; Fedorovich and

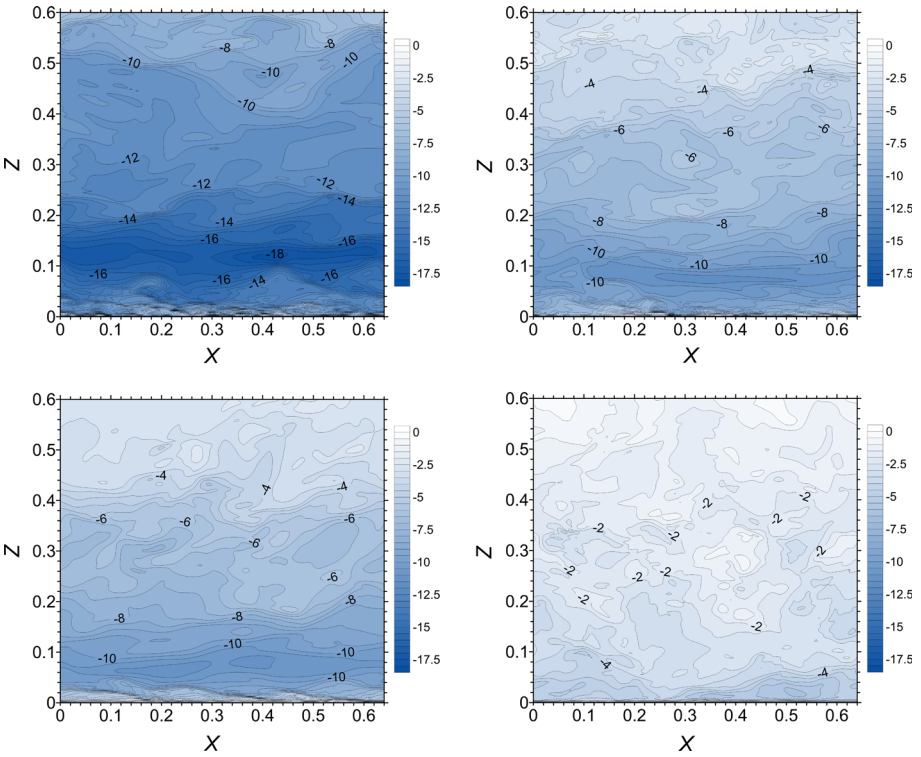

Fig. 2 Central $X-Z$-plane cross-sections of the along-slope (U) velocity field in simulated katabatic flows with $\alpha = 2.5°$ at $T = 652$ s (*top left*), $\alpha = 5°$ at $T = 850$ s (*top right*), $\alpha = 10°$ at $T = 412$ s (*bottom left*), and $\alpha = 20°$ at $T = 220$ s (*bottom right*). Coordinates are expressed in m, U in m s^{-1}

Shapiro 2009a; Axelsen and van Dop 2009a, b; Chemel et al. 2009; Burkholder et al. 2011; Largeron et al. 2013).

The scaled boundary-layer problem incorporates the following differential equations,

$$\frac{\partial u}{\partial t} + Re_W \left(u\frac{\partial u}{\partial x} + v\frac{\partial u}{\partial y} + w\frac{\partial u}{\partial z} \right) = -\frac{\partial \pi}{\partial x} + b + \frac{\partial^2 u}{\partial z^2}, \tag{10}$$

$$\frac{\partial v}{\partial t} + Re_W \left(u\frac{\partial v}{\partial x} + v\frac{\partial v}{\partial y} + w\frac{\partial v}{\partial z} \right) = -\frac{\partial \pi}{\partial y} + \frac{\partial^2 v}{\partial z^2}, \tag{11}$$

$$0 = -\frac{\partial \pi}{\partial z} + b, \tag{12}$$

$$Pr\frac{\partial b}{\partial t} + Pr\,Re_W \left(u\frac{\partial b}{\partial x} + v\frac{\partial b}{\partial y} + w\frac{\partial b}{\partial z} \right) = -u - w + \frac{\partial^2 b}{\partial z^2}, \tag{13}$$

$$\frac{\partial u}{\partial x} + \frac{\partial v}{\partial y} + \frac{\partial w}{\partial z} = 0, \tag{14}$$

where Re_W is a W-scale-based Reynolds number

$$\mathrm{Re}_W \equiv \frac{W_s Z_s}{\nu} = Re_U \tan\alpha = \frac{B_s \sin^{1/2}\alpha}{Pr^{3/4}\nu^{1/2}N^{3/2}\cos\alpha}, \tag{15}$$

and the boundary conditions

$$\lim_{z\to\infty}(u,\ v,\ w,\ b,\ \pi) = 0, \tag{16}$$

$$u|_{z=0} = v|_{z=0} = w|_{z=0} = 0, \tag{17}$$

$$b|_{z=0} = -1, \ \text{(if the buoyancy is specified)}, \tag{18a}$$

$$\left.\frac{\partial b}{\partial z}\right|_{z=0} = -1, \ \text{(if the buoyancy flux is specified)}. \tag{18b}$$

We thus see that the scaled boundary-layer problem is governed by just two parameters: Pr and Re_W. The slope angle α has been removed as an independent governing parameter and appears only as a stretching factor in the scales (7b) and (9), and in the definition of Re_W. Had we used (7a), (7b) and (9) to scale the original problem, we would have obtained a dimensionless problem involving three governing parameters: α, Pr, and Re_W (or Re_U). We also would have obtained a three-parameter problem if scalings other than (7a), (7b) and (9) had been applied to the boundary-layer problem, for example, if W_s had been defined to be the same as U_s.

The preceding analysis leads us to offer a boundary-layer scaling hypothesis: the full katabatic-wind problem of Sect. 2 is essentially a two-parameter rather than three-parameter problem. Specifically, when non-dimensionalized using the boundary-layer scalings (7a), (7b) and (9), the solutions of the full katabatic-wind problem should essentially depend only on Re_W and Pr; the scaled solution curves for the full problem should be largely independent of slope angle.

4 Testing the Boundary-Layer Hypothesis

Since ν and κ in our study are intended to be molecular coefficients, and such coefficients have only a weak temperature dependence at normal atmospheric conditions (Kundu and Cohen 2002), the Prandtl number can basically be regarded as fixed. In this case, our boundary-layer scaling hypothesis is that the solution of the full katabatic-wind problem, when scaled with (7a), (7b) and (9), is a function only of Re_W. One may speculate that, for large enough Re_W, the solution curves become independent of Re_W, but questions about the asymptotic behaviour of the flow are beyond the scope of the present investigation.

We test the above scaling hypothesis by solving (2) to (6) using DNS for the surface flux-forced case (7b) with different sets of values of α, ν, N, and B_s constrained by (15) to yield the same Re_W. Unfortunately, because of the heavy computational requirements imposed by DNS and the need to run shallow slope simulations over very long periods of time (since the frequency of oscillations varies as $\sin\alpha$), it was not possible to explore the Re_W dependence of the solution. Here, we fix the Prandtl number at $Pr = 1$ and the Reynolds number at $Re_W = 4{,}243$, and vary α, ν, N, and B_s (through F_s in (7b)) as indicated in

Table 1 Governing parameters used in the DNS of katabatic flows for a fixed Reynolds number ($Re_W = 4{,}243$) and Prandtl number ($Pr = 1$)

Simulation	α (degrees)	$\nu(=\kappa)$ (m^2 s^{-1})	N (s^{-1})	F_s (m^2 s^{-3})
Case 1	2.5	10^{-4}	1.19	−0.6
Case 2	5	10^{-4}	0.842	−0.3
Case 3	10	2×10^{-4}	0.599	−0.3
Case 4	20	10^{-4}	0.868	−0.3

Table 1. Because only one Reynolds number was considered, and it was relatively small, the validation of our scaling hypothesis should be regarded as very preliminary.

The employed DNS procedures are similar to those described in Fedorovich and Shapiro (2009a, b). The prognostic variables (U, V, W, and B) are updated with a hybrid leapfrog/Adams-Moulton third-order timestepping scheme. Spatial derivatives are discretized using second-order finite-difference expressions on a staggered slope-following Cartesian grid. On the surface we impose no-slip and impermeability conditions, and specify the buoyancy flux F_s. Periodic conditions are imposed in the X and Y directions, and zero normal-gradient conditions are imposed at the top of the domain. The normalized pressure perturbation is obtained from the Poisson equation that results from taking the divergence of the equations of motion. The Poisson solver uses fast Fourier transforms over $X - Y$ planes and a tridiagonal matrix inversion in the Z direction. The surface condition for pressure is the Neumann condition inferred from the slope-normal equation of motion.

The computational grid consisted of 128×128 points on $X - Y$ planes and 1000 points in the Z direction, with grid spacings of $\Delta X = \Delta Y = 0.005$ m and $\Delta Z = 0.003$ m, which roughly satisfy the spacing requirements for resolved DNS given the values of the flow-controlling parameters indicated in Table 1 (Fedorovich and Shapiro 2009a, b). Each simulation was run for the duration of at least five oscillations. The simulation with the smallest angle, Case 1, required over six months of computing time to encompass five oscillations. The other cases required less computing time per oscillation, and were run out to as many as ten oscillations.

Sample cross-sections of the dimensional U and B fields for the four cases are depicted in Figs. 2 and 3 for a lower portion of the computational domain that partially contains the momentum boundary layer and fully contains the (much shallower) thermal boundary layer.[4] Both the intensity and depth of the boundary layers vary significantly between the four cases, with the greatest depth obtained, as in the Prandtl theory, for the smallest slope angle. Consistent with our expectations regarding the anisotropy of flow structures in stably stratified flows, many (though not all) of the small-scale features evident in these figures tend to be elongated in the along-slope direction.

The evolution of the dimensional (U) and scaled (u) velocity components, averaged over $X - Y$ planes, is shown in Figs. 4 and 5, respectively. The corresponding evolution of the dimensional (B) and scaled (b) buoyancy fields is shown in Figs. 6 and 7. To facilitate comparisons between the four cases, the presentations are truncated at a common dimensional time in Figs. 4 and 6, and a common non-dimensional time in Figs. 5 and 7 (for example, only

[4] Results are shown at the (uncoordinated) terminal times of the individual simulations. In general, the end times correspond to different phases of the temporal oscillation. However, the amplitudes of the velocity and buoyancy oscillations decay with time and are small fractions of the mean characteristic velocity and thermal disturbances at these later times.

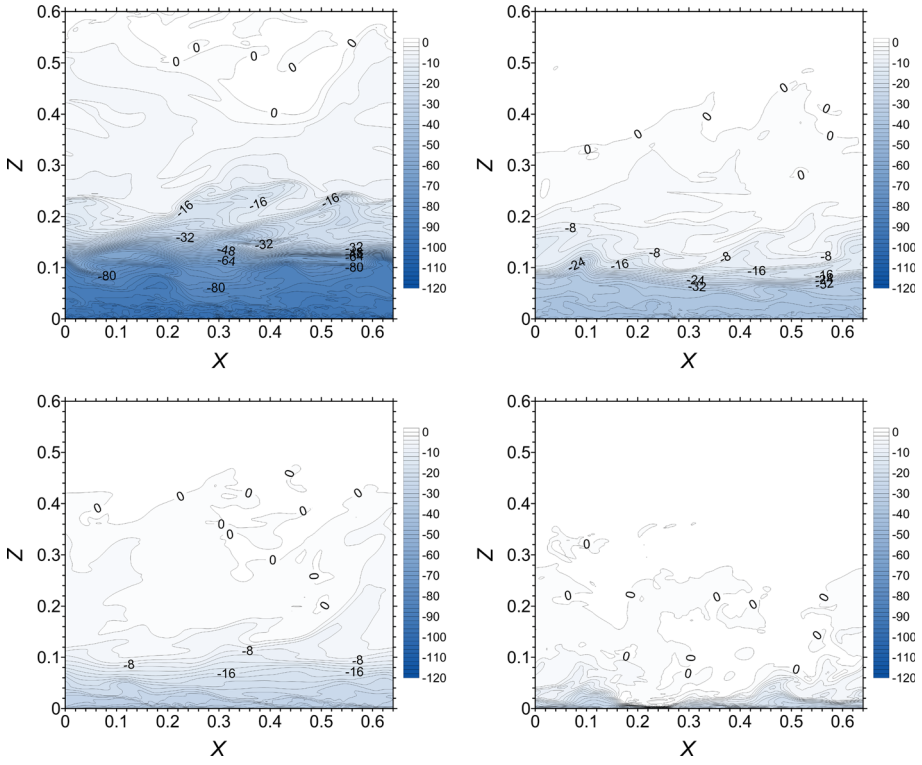

Fig. 3 Central $X-Z$-plane cross-sections of the buoyancy field B in simulated katabatic flows with $\alpha = 2.5°$ at $T = 652$ s (*top left*), $\alpha = 5°$ at $T = 850$ s (*top right*), $\alpha = 10°$ at $T = 412$ s (*bottom left*), and $\alpha = 20°$ at $T = 220$ s (*bottom right*). Coordinates are expressed in m, B in m s^{-2}

the first of five simulated oscillations appears for Case 1 in the top left panels of Figs. 4 and 6). Large differences between the four cases are seen in the dimensional intensity and depth of the katabatic jet in Fig. 4, and in the dimensional intensity and depth of the thermal boundary layer in Fig. 6. In contrast, the corresponding scaled fields are much more similar (Fig. 5 vs. 4, and Fig. 7 vs. 6). We also see that the large differences in the dimensional oscillation periods (one, two, three, and ten periods) are greatly reduced when expressed in scaled time (approximately five oscillations in all panels of Figs. 5 and 7, with the oscillations most apparent in Fig. 7). Since the planar-averaged fields depicted in these figures still appear fairly noisy, we did not explore the extent to which the higher-order turbulence statistics follow scaling laws inferred from (9).

Figures 4 and 6 also show that the dimensional momentum boundary layer is much thicker than its thermal counterpart.[5] Qualitatively similar results are evident in recent DNS and LES studies of Prandtl-like katabatic flows (DNS: Fedorovich and Shapiro 2009a; LES: Axelsen and van Dop 2009b and Burkholder et al. 2011), in a LES of katabatic flow down a symmetric mountain ridge with planar slopes (Smith and Skyllingstad 2005), and in a LES of katabatic flow in a two-dimensional periodic mountain-valley system (Smith and Porté-Agel 2013). A

[5] For the purpose of the present discussion we define the boundary-layer depths for momentum and buoyancy loosely as the heights at which the magnitudes of the downslope velocity and buoyancy are reduced to some small percentage (say, 10 %) of their peak magnitudes.

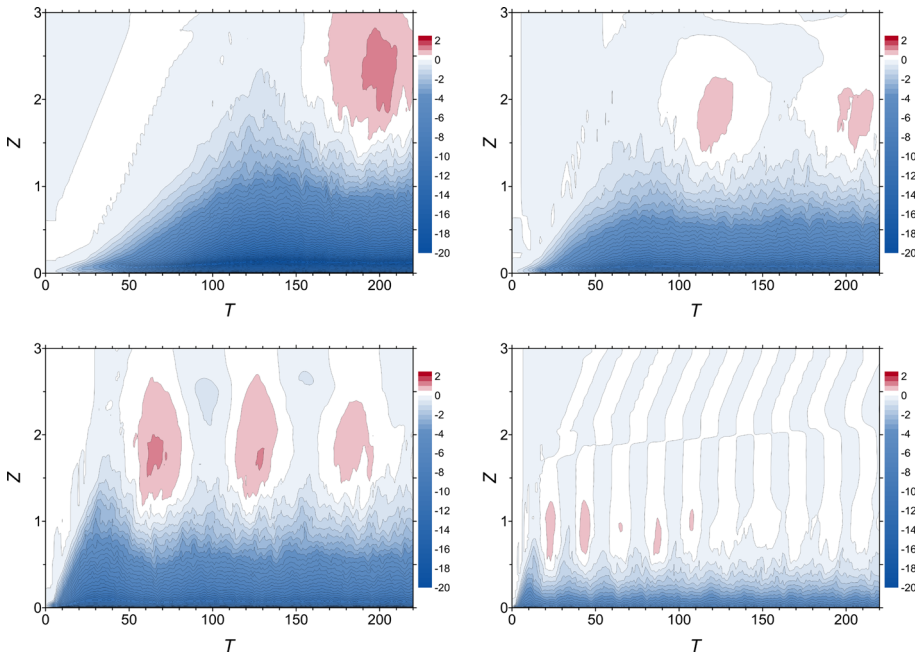

Fig. 4 Evolution of the $X-Y$ plane-averaged dimensional along-slope velocity component (U) for $\alpha = 2.5°$ (*top left*), $\alpha = 5°$ (*top right*), $\alpha = 10°$ (*bottom left*), and $\alpha = 20°$ (*bottom right*). T is in s, U is in m s^{-1}

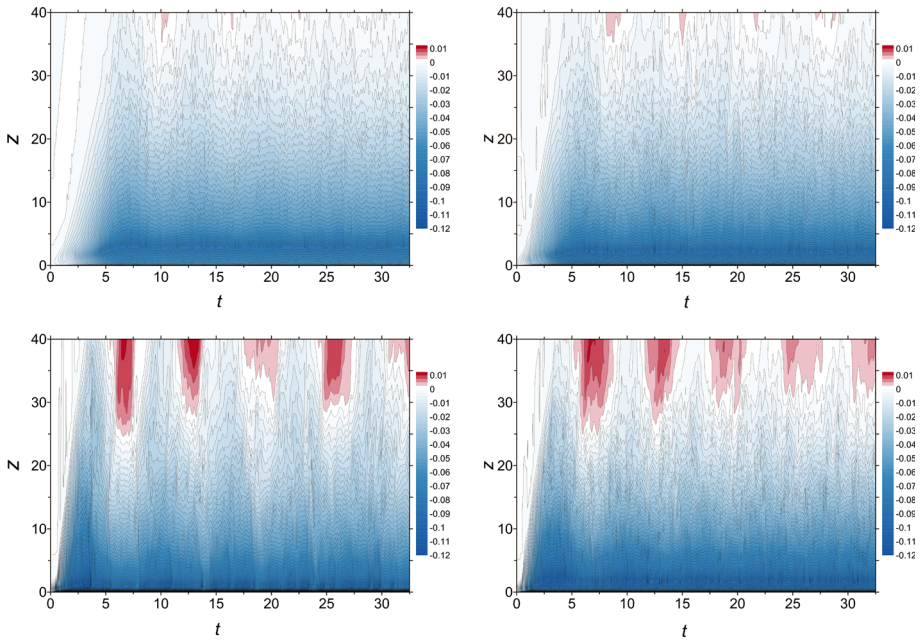

Fig. 5 Evolution of the $X-Y$ plane-averaged scaled along-slope velocity component (u) for $\alpha = 2.5°$ (*top left*), $\alpha = 5°$ (*top right*), $\alpha = 10°$ (*bottom left*), and $\alpha = 20°$ (*bottom right*)

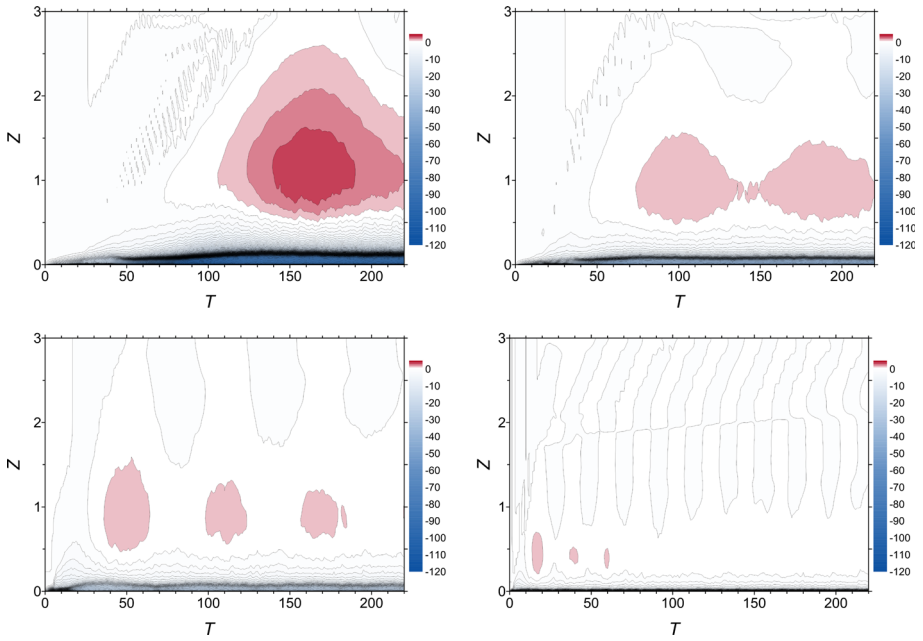

Fig. 6 Evolution of the $X - Y$ plane-averaged dimensional buoyancy (B) for $\alpha = 2.5°$ (*top left*), $\alpha = 5°$ (*top right*), $\alpha = 10°$ (*bottom left*), and $\alpha = 20°$ (*bottom right*). T is in s, B is in m s^{-2}

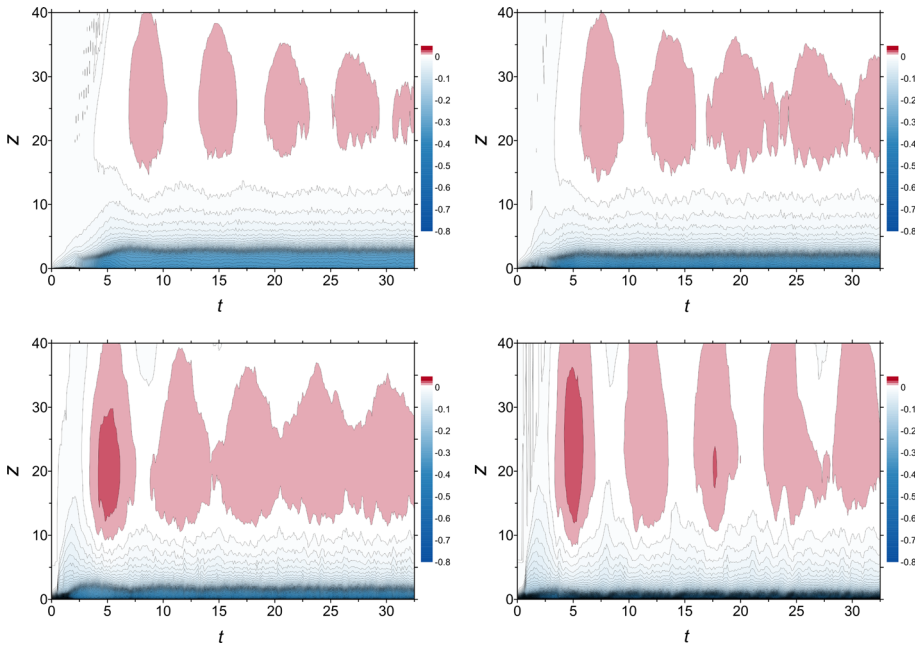

Fig. 7 Evolution of the $X - Y$ plane-averaged scaled buoyancy (b) for $\alpha = 2.5°$ (*top left*), $\alpha = 5°$ (*top right*), $\alpha = 10°$ (*bottom left*), and $\alpha = 20°$ (*bottom right*)

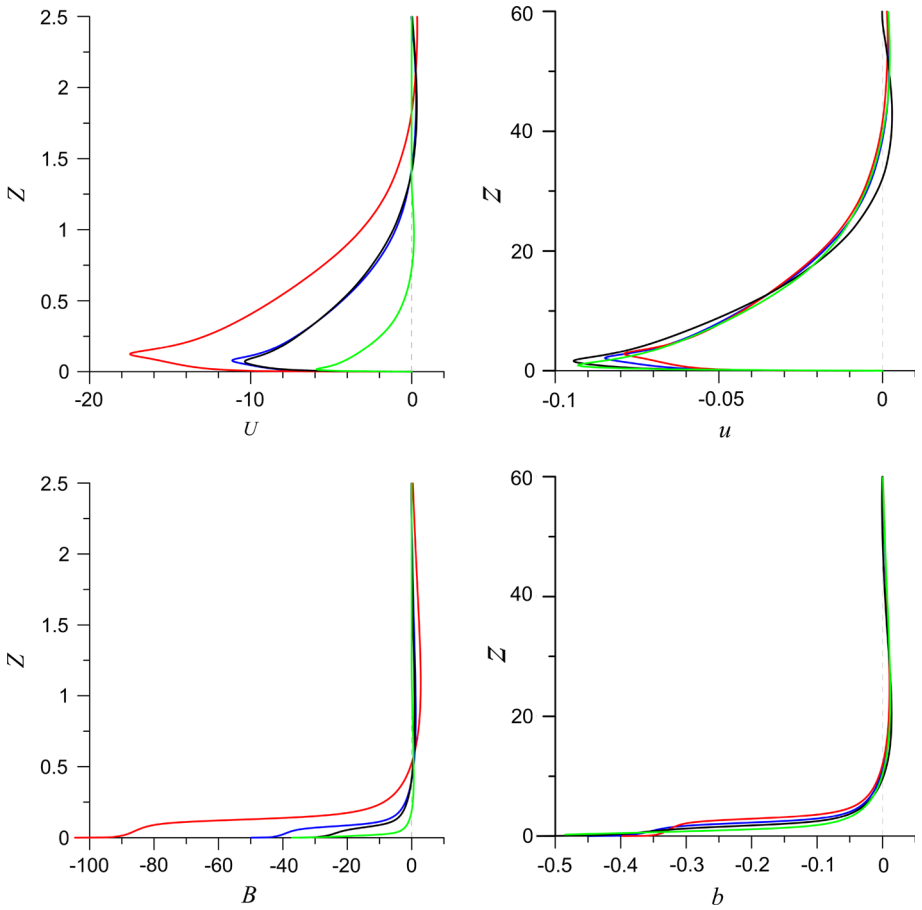

Fig. 8 Mean (averaged in time and over $X - Y$ planes) profiles of the along-slope velocity component (dimensional U, scaled u) and buoyancy (dimensional B, scaled b) in simulated katabatic flows with Re_W (= 4,243) and Pr (= 1), for the parameter combinations given in Table 1: Case 1 (*red line*), Case 2 (*blue line*), Case 3 (*black line*) and Case 4 (*green line*)

similar result is also evident in plots of tower data presented in the latter study. Consistent with the Prandtl theory, weak return flow is found above the primary katabatic jet (upper part of panels in Figs. 4 and 5), and small positive buoyancies are found above the cold thermal boundary layer (middle and upper parts of panels in Figs. 6 and 7).

Finally, we consider the mean (averaged in time over several oscillations and in space over $X - Y$ planes) profiles of the dimensional and non-dimensional along-slope velocity and buoyancy fields (Fig. 8). This figure shows that the large spread among the four dimensional (U) profiles is greatly reduced in the corresponding scaled (u) profiles. A similarly dramatic reduction of spread is seen between the dimensional (B) and scaled (b) buoyancy profiles.

An additional simulation (not shown) was performed with a slope angle of $\alpha = 1.25°$. Faced with the extreme computational burden associated with this very small angle, we ran the simulation in a domain consisting of 64×64 points on $X - Y$ planes, which was four times smaller than was used in Cases 1–4. Consistent with the scaling hypothesis, the scaled wind and buoyancy profiles in this case again tend to collapse on the other scaled profiles. However,

the depth of the scaled thermal boundary layer, as defined by the location of an inflection point, was somewhat larger than would be expected if there existed a tendency for results from successively smaller slope angle simulations to converge. Although we cannot rule out that some of the differences were due to differences in domain size, another possibility is that a deepening of the dimensional thermal boundary layer with decreasing slope angle (consistent with Prandtl's theory and our DNS results) reduced the boundary-layer-like character of the flow. Indeed, in the case of a zero slope angle, the concept of a katabatic boundary layer breaks down.

5 Summary and Conclusions

The Prandtl model setting of flow of a viscous stably stratified fluid along a uniformly cooled planar slope has provided a particularly simple framework for our study of scaling relationships in turbulent katabatic flows. Motivated by studies suggesting that flow anisotropies in stably stratified flows could extend over the major portion of the spectral range of turbulent motions, we exploited a boundary-layer-approximated governing equation set to develop such relationships. The scaled boundary-layer problem was controlled by just two parameters: the Prandtl number Pr and a Reynolds number Re_W. The slope angle did not appear as an independent parameter, but merely served as a stretching factor in the scales for the dependent and independent variables and appeared in the Reynolds number. Based on our analysis of the boundary-layer problem, we hypothesized that the full katabatic-flow problem, non-dimensionalized using the deduced scales, would be largely controlled by just Pr and Re_W.

The scaling hypothesis was tested using DNS of katabatic flow with four different sets of values for slope angle, viscosity, Brunt-Väisälä frequency, and surface buoyancy flux, with values constrained to yield fixed values of Pr $(= 1)$ and Re_W $(= 4{,}243)$. The mean-profile results from these single Pr–Re_W experiments were very encouraging, and suggested that the hypothesis may have merit. We hasten to note, however, that since the results were obtained for just one Reynolds number, one that was much smaller than would be typical of a real katabatic flow, our results should be regarded as very preliminary. If the hypothesis can be confirmed for larger Reynolds numbers, it would have the potential to yield significant computational savings in future parametric studies of Prandtl-type turbulent katabatic flows.

References

Adolphs U, Wendler G (1995) A pilot study on the interactions between katabatic winds and polynyas at the Adélie Coast, eastern Antarctica. Antarct Sci 7:307–314

Atkinson BW (1981) Meso-scale atmospheric circulations. Academic Press, London, 495 pp

Axelsen SL, Dop H (2009a) Large-eddy simulation of katabatic winds. Part 1: comparison with observations. Acta Geophys 57:803–836

Axelsen SL, van Dop H (2009b) Large-eddy simulation of katabatic winds. Part 2: sensitivity study and comparison with analytical models. Acta Geophys 57:837–856

Barthélemy A, Hugues G, Mathiot P, Fichefet T (2012) Inclusion of a katabatic wind correction in a coarse-resolution global coupled climate model. Ocean Model 48:45–54

Bastin S, Drobinski P (2005) Temperature and wind velocity oscillations along a gentle slope during sea-breeze events. Boundary-Layer Meteorol 114:573–594

Bejan A (2013) Convection heat transfer. Wiley, Hoboken, 696 pp

Brazel AJ, Fernando HJS, Hunt JCR, Selover N, Hedquist BC, Pardyjak E (2005) Evening transition observations in Phoenix, Arizona. J Appl Meteorol 44:99–112

Bromwich DH, Kurtz DD (1984) Katabatic wind forcing of the Terra Nova Bay polynya. J Geophys Res 89:3561–3572
Bromwich DH (1989) Satellite analyses of Antarctic katabatic wind behavior. Bull Am Meteorol Soc 70:738–749
Bromwich D, Liu Z, Rogers AN, Van Woert ML (1998) Winter atmospheric forcing of the Ross Sea polynya. In: Jacobs SS, Weiss RF (eds) Ocean, ice, and atmosphere: interactions at the Antarctic continental margin, Antarctic research series, vol 75. American Geophysical Union, Washington, pp 101–133
Burkholder B, Fedorovich E, Shapiro A (2011) Evaluating sub-grid scale models for large-eddy simulation of turbulent katabatic flow. Quality and reliability of large-eddy simulations II. Springer, Dordrecht, pp 149–160
Chemel C, Staquet C, Largeron Y (2009) Generation of internal gravity waves by a katabatic wind in an idealized alpine valley. Meteorol Atmos Phys 103:187–194
Clements WE, Archuleta JA, Hoard DE (1989) Mean structure of the nocturnal drainage flow in a deep valley. J Appl Meteorol 28:457–462
Cotton JH, Michael KJ (1994) The monitoring of katabatic wind-coastal polynya interaction using AVHRR imagery. Antarct Sci 6:537–540
Defant F (1949) Zur Theorie der Hangwinde, nebst Bemerkungen zur Theorie der Berg- und Talwinde. Arch Meteorol Geophys Bioklim Ser A 1:421–450
Egger J (1990) Thermally forced flows: theory. In: Blumen W (ed) Atmospheric processes over complex terrain, vol 45. Meteorological Monographs. American Meteorological Society, Boston, pp 43–58
Fedorovich E, Shapiro A (2009a) Structure of numerically simulated katabatic and anabatic flows along steep slopes. Acta Geophys 57:981–1010
Fedorovich E, Shapiro A (2009b) Turbulent natural convection along a vertical plate immersed in a stably stratified fluid. J Fluid Mech 636:41–57
Fernando HJS (2010) Fluid dynamics of urban atmospheres in complex terrain. Annu Rev Fluid Mech 42:365–389
Fernando HJS, Lee SM, Anderson J, Princevac M, Pardyjak E, Grossman-Clarke S (2001) Urban fluid mechanics: air circulation and contaminant dispersion in cities. Environ Fluid Mech 1:107–164
Gallee H, Schayes G (1994) Development of a 3-dimensional meso-γ primitive equation model: katabatic winds simulation in the area of Terra Nova Bay, Antarctica. Mon Weather Rev 122:671–685
Godeferd FS, Staquet C (2003) Statistical modelling and direct numerical simulations of decaying stably stratified turbulence. Part 2. Large-scale and small-scale anisotropy. J Fluid Mech 486:115–159
Grisogono B, Oerlemans J (2001) Katabatic flow: analytic solution for gradually varying eddy diffusivities. J Atmos Sci 58:3349–3354
Grisogono B, Oerlemans J (2002) Justifying the WKB approximation in pure katabatic flows. Tellus 54A:453–462
Grisogono B, Axelsen SL (2012) A note on the pure katabatic wind maximum over gentle slopes. Boundary-Layer Meteorol 145:527–538
Heinemann G, Klein T (2002) Modelling and observations of the katabatic flow dynamics over Greenland. Tellus 54A:542–554
Hootman BW, Blumen W (1983) Analysis of nighttime drainage winds in Boulder, Colorado during 1980. Mon Weather Rev 111:1052–1061
Hopfinger EJ (1987) Turbulence in stratified fluids: a review. J Geophys Res 92:5287–5303
Hunt JCR, Fernando HJS, Princevac M (2003) Unsteady thermally driven flows on gentle slopes. J Atmos Sci 60:2169–2182
Jiménez MA, Cuxart J (2005) Large-eddy simulations of the stable boundary layer using the standard Kolmogorov theory: range of applicability. Boundary-Layer Meteorol 115:241–261
Kundu PK, Cohen IM (2002) Fluid mechanics, 2nd edn. Academic Press, San Diego, 730 pp
Langhaar HL (1951) Dimensional analysis and theory of models. Wiley, New York, 166 pp
Largeron Y, Staquet C, Chemel C (2013) Characterization of oscillatory motions in the stable atmosphere of a deep valley. Boundary-Layer Meteorol 148:439–454
Lee SM, Fernando HJS, Princevac M, Zajic D, Sinesi M, McCulley JL, Anderson J (2003) Transport and diffusion of ozone in the nocturnal and morning planetary boundary layer of the Phoenix valley. Environ Fluid Mech 3:331–362
Lindborg E (2006) The energy cascade in a strongly stratified fluid. J Fluid Mech 550:207–242
Lu R, Turco RP (1994) Air pollutant transport in a coastal environment. Part I: two-dimensional simulations of sea-breeze and mountain effects. J Atmos Sci 51:2285–2308
Mahrt L (1998) Stratified atmospheric boundary layers and breakdown of models. Theor Comput Fluid Dyn 11:263–279

Massom RA, Harris PT, Michael KJ, Potter MJ (1998) The distribution and formative processes of latent-heat polynyas in East Antarctica. Ann Glaciol 27:420–426
Mauritsen T, Svensson G, Zilitinkevich SS, Esau I, Enger L, Grisogono B (2007) A total turbulent energy closure model for neutrally and stably stratified atmospheric boundary layers. J Atmos Sci 64:4113–4126
McNider RT (1982) A note on velocity fluctuations in drainage flows. J Atmos Sci 39:1658–1660
Mo R (2013) On adding thermodynamic damping mechanisms to refine two classical models of katabatic winds. J Atmos Sci 70:2325–2334
Noppel H, Fiedler F (2002) Mesoscale heat transport over complex terrain by slope winds: a conceptual model and numerical simulations. Boundary-Layer Meteorol 104:73–97
Oerlemans J (1998) The atmospheric boundary layer over melting glaciers. In: Holtslag AAM, Duynkerke PG (eds) Clear and cloudy boundary layers. Royal Netherlands Academy of Arts and Sciences, Amsterdam, pp 129–153
Oerlemans J, Grisogono B (2002) Glacier winds and parameterisation of the related surface heat fluxes. Tellus A 54:440–452
Ohshima KI, Fukamachi Y, Williams GD, Nihashi S, Roquet F, Kitade Y, Tamura T, Hirano D, Field I, Hindell MA, Aoki S, Wakatsuchi M (2013) Antarctic bottom water production by intense sea-ice formation in the Cape Darnley polynya. Nat Geosci 6:235–240
Papadopoulos KH, Helmis CG, Soilemes AT, Kalogiros J, Papageorgas PG, Asimakopoulos DN (1997) The structure of katabatic flows down a simple slope. Q J R Meteorol Soc 123:1581–1601
Parish TP, Waight KT (1987) The forcing of antarctic katabatic winds. Mon Weather Rev 115:2214–2226
Parish TP (1992) On the role of Antarctic katabatic winds in forcing large-scale tropospheric motions. J Atmos Sci 49:1374–1385
Parmhed O, Oerlemans J, Grisogono B (2004) Describing surface fluxes in katabatic flow on Breidamerkurjökull, Iceland. Q J R Meteorol Soc 130:1137–1151
Pettersson Reif BA, Andreassen Ø (2003) On local isotropy in stratified homogeneous turbulence. SIAM J Appl Math 64:309–321
Pope SB (2000) Turbulent flows. Cambridge University Press, UK, 771 pp
Poulos G, Zhong S (2008) An observational history of small-scale katabatic winds in mid-latitudes. Geogr Compass 2:1798–1821
Princevac M, Hunt JCR, Fernando HJS (2008) Quasi-steady katabatic winds on slopes in wide valleys: hydraulic theory and observations. J Atmos Sci 65:627–643
Prandtl L (1942) Führer durch die Strömungslehre. Vieweg and Sohn, Braunschweig, 648 pp
Raga GB, Baumgardner D, Kok G, Rosas I (1999) Some aspects of boundary layer evolution in Mexico City. Atmos Environ 33:5013–5021
Renfrew IA (2004) The dynamics of idealized katabatic flow over a moderate slope and ice shelf. Q J R Meteorol Soc 130:1023–1045
Renfrew IA, Anderson PS (2006) Profiles of katabatic flow in summer and winter over Coats Land, Antarctica. Q J R Meteorol Soc 132:779–802
Riley JJ, Lelong M-P (2000) Fluid motions in the presence of strong stable stratification. Annu Rev Fluid Mech 32:613–657
Schumann U (1990) Large-eddy simulation of the up-slope boundary layer. Q J R Meteorol Soc 116:637–670
Shapiro A, Fedorovich E (2007) Katabatic flow along a differentially-cooled sloping surface. J Fluid Mech 571:149–175
Shapiro A, Burkholder B, Fedorovich E (2012) Analytical and numerical investigation of two-dimensional katabatic flow resulting from local surface cooling. Boundary-Layer Meteorol 145:249–272
Smith CM, Porté-Agel F (2013) Comparison of subgrid models for large-eddy simulation of katabatic flows. Q J R Meteorol Soc. doi:10.1002/qj.2212
Smith CM, Skyllingstad ED (2005) Numerical simulation of katabatic flow with changing slope angle. Mon Weather Rev 133:3065–3080
Steyn DG, De Wekker SFJ, Kossmann M, Martilli A (2012) Boundary layers and air quality in mountainous terrain. In: Chow FK, De Wekker SFJ, Snyder BJ (eds) Mountain weather research and forecasting: recent progress and current challenges. Springer, Dordrecht, pp 261–289
Thoroddsen ST, Van Atta CW (1992) The influence of stable stratification on small-scale anisotropy and dissipation in turbulence. J Geophys Res 97:3647–3658
Thoroddsen ST, Van Atta CW (1996) Experiments on density-gradient anisotropies and scalar dissipation of turbulence in a stably stratified fluid. J Fluid Mech 322:383–409
Tyson PD (1968) Velocity fluctuations in the mountain wind. J Atmos Sci 25:381–384
Van Woert ML (1999) Wintertime dynamics of the Terra Nova Bay polynya. J Geophys Res 104:7753–7769
Waite ML, Bartello P (2004) Stratified turbulence dominated by vortical motion. J Fluid Mech 517:281–308
Werne J, Fritts DC (2001) Anisotropy in a stratified shear layer. Phys Chem Earth (B) 26:263–268

Whiteman CD (1990) Observations of thermally developed wind systems in mountainous terrain. In: Blumen W (ed) Atmospheric processes over complex terrain, vol 45. Meteorological Monographs. American Meteorological Society, Boston, pp 5–42

Whiteman CD (2000) Mountain meteorology: fundamentals and applications. Oxford University Press, New York, 355 pp

Williams GD, Aoki S, Jacobs SS, Rintoul SR, Tamura T, Bindoff NL (2010) Antarctic Bottom Water from the Adélie and George V Land coast, East Antarctica (140–149°E). J Geophys Res 115:C04027. doi:10.1029/2009JC005812

Wong ABD, Griffiths RW (1999) Stratification and convection produced by multiple turbulent plumes. Dyn Atmos Oceans 30:101–123

Zammett RJ, Fowler AC (2007) Katabatic winds on ice sheets: a refinement of the Prandtl model. J Atmos Sci 64:2707–2716

Zardi D, Whiteman CD (2012) Diurnal mountain wind systems. In: Chow FK, De Wekker SFJ, Snyder BJ (eds) Mountain weather research and forecasting: recent progress and current challenges. Springer, Dordrecht, pp 35–119